SUPPLEMENT MATERIAL

Title: Transmural Dispersion of Repolarization in Failing and Non Failing Human Ventricle

Authors: Alexey V. Glukhov, Ph.D.; Vadim V. Fedorov, Ph.D.; Qing Lou, B.S.; Vinod K. Ravikumar; Paul W. Kalish; Richard B. Schuessler, Ph.D.; Nader Moazami, M.D.; Igor R. Efimov, PhD.

METHODS

Patients groups

Cardiomyopathic failing hearts (n=5) were obtained during transplantation at the Barnes-Jewish Hospital, Washington University in Saint Louis, MO. As a control, we used non-failing donor hearts (n=5), which were rejected for transplantation for various reasons, including age, early stage hypertrophy, atrial fibrillation, and coronary disease. Ejection fraction values were obtained immediately before heart removal from the patient chest and could reflect the effect of patient reanimation. Nevertheless, all non-failing hearts were characterized as hearts without history of heart failure. Donor hearts were provided by the Mid-America Transplant Services (Saint Louis, MO). **Online Table I** presents clinical characteristics of non-failing human hearts. In hearts #1 and #4, the early stage of hypertrophy was observed which together with the patient age have an effect on the heart electrophysiology. However, we did no observe any deviations in

these hearts compared with another non-failing hearts (data from non-failing heart #4 is presented on **Online Figures II - IV**). Acute cardiac ischemia as well as a presence of atrial fibrillation in heart #2 were caused by resuscitation of the patient and were not chronical (data from non-failing heart #2 is presented on **Online Figures III and IV**, and did not differ from another non-failing hearts). Non-failing heart #5 was obtained from the patient who died from the overdose of Tylenol which could affect on the cardiac electrophysiology and induced more distinguished islands of M-cell in this heart (**Figures 2, 3, 5-7 and Online Figures II and III**).

Experimental preparation: Quality of perfusion

We isolated wedges of the human ventricular wall as previously described in canine heart.[1, 2] Briefly, after harvesting, the hearts were immediately perfused through the aorta with a cardioplegic solution. The cardioplegic perfusion washed out the blood and protected the hearts during the subsequent period of wedge isolation. We then isolated a transmural wedge from the posterior-lateral part of left ventricular (LV) free wall. The thickness of the LV was not differ between non-failing and failing wedge preparations (16.6±1.4 mm vs 19.2±1.5 mm, respectively, p=0.26). Data from the each heart are presented in **Online Table III**. The preparation was dissected several centimeters below the base of the ventricles and extended about 3 cm towards the apex. All preparations were dissected approximately from the same area of the hearts with the regard for the quality of perfusion.

Before dissection, the quality of perfusion was verified by injection of Methylene Blue dye (Sigma, St. Louis, MO). Based on the blue color in areas supplied by solution, the appropriate preparation was selected. Each wedge contained a section of coronary artery (diameter: ≥1 mm) along its length, which was cannulated with the flexible plastic cannula custom made for these experiments. The quality of perfusion of the dissected preparation was also verified by injection of Methylene Blue dye. Poorly perfused tissue was trimmed from the wedges. Major arterial leaks in the wedges were ligated with silk suture. The isolated tissues were mounted in a warm chamber with the dissected exposed transmural surface up, facing the optical apparatus. The preparation was both superfused and coronary perfused Tyrode solution. We maintained 37°C and an arterial pressure of 60–70 mmHg. The preparation was fully immersed in the perfusion efflux, which assured appropriate superfusion.

After 20-30 minutes of washout, gradual warming after cold cardioplegia to 37^{o}C, tissue recovery, and stabilization, the wedges were stained with 4 μM of membrane potential-sensitive fluorescent dye di-4-ANEPPS (Molecular Probes, Eugene, OR). The dye staining was possible only in well-perfused areas of the preparation which was an additional verification of quality of adequate tissue perfusion. The optical field of view was selected so as to avoid the areas with low fluorescent signal.

Data processing and analyzing

A custom-made Matlab-based computer program was used to analyze APs offline.[3] First, the signals were filtered using the low-pass Butterworth filter at 50 Hz. Activation maps were constructed from activation times, which were determined from the dV/dt_{max} in each channel. Finally, AP duration was calculated as time difference between the activation time (dV/dt_{max}) and 80% of repolarization (APD80).

Online Figure IV represents four examples of activation and APD distribution contour maps. Conduction velocity was calculated as the maximal velocity in the endocardium-epicardium direction. Because of the endocardial pacing, it was not possible to quantify conduction velocity in transversal direction of excitation propagation as well as its anisotropy. We also did not test an effect of different pacing sites on the APD distribution pattern and transmural conduction as proposed in other studies.[4]

APD for sub-endocardial and sub-epicardial layers were calculated by the averaging of maximal values of the first several pixels (before any significant APD changes) from the each side respectively to resolve the presence of M-cell islands. Transmural APD gradient was calculated as the difference between maximal and minimal values of APD through the transmural cross-section of LV (**Online Figure IV**).

Local APD gradient was measured by $\left(\left(\frac{\mathbf{d(APD)}}{\mathbf{d}x}\right)^2+\left(\frac{\mathbf{d(APD)}}{\mathbf{d}y}\right)^2\right)^{\frac{1}{2}}$, where *x* and *y* were the directions of rows and columns of pixels. $\frac{\mathbf{d(APD)}}{\mathbf{d}x}$ or $\frac{\mathbf{d(APD)}}{\mathbf{d}y}$ was estimated by APD difference of neighboring pixels over the length of a pixel. To reduce the sensitivity to noise, APD map was first filtered by a 3 by 3 averaging filter before the estimation. To estimate the size and area of islands with prolonged APD (shown in brown color on panels C of **Online Figure II**), we used the following steps. First, region with APD within the top 30% range was identified. That is, APD cut-off threshold was calculated by [APD_{max}-0.3×(APD_{max}-APD_{min})]. The qualified areas were marked by dotted lines on **Online Figure II.** Second, local APD gradient distributions were calculated in these areas (see **Online Figure II B)**. Threshold of 15 mm/ms was used to identify the high-APD-gradient boundary around the island with prolonged repolarization (dark red color on panels B). After then, maximum APD within this local APD gradient boundary was identified and then used as a threshold for island with prolonged repolarization. APD threshold was individual for each particular island (see **Online Figure II C)**. The area of the island was then calculated as a product of number of pixels within the island and the size of a single pixel (see **Online Figure II C)**.

Microelectrode recordings: Effect of Blebbistatin

To immobilize the preparation, we used the excitation-contraction uncoupler Blebbistatin (BB, 10 μM).[5-7] The glass microelectrode technique was used to

validate optical action potentials and effect of Blebbistatin on action potential morphology in the isolated coronary-perfused preparation (**Online Figure I A**) as described earlier. Transmembrane potentials were recorded at 5 kHz by conventional glass microelectrodes filled with 3 M KCl-filled glass microelectrodes with 15- to 25 MΩ resistance. As shown in **Online Figure I B**, in the failing human LV wedge preparation, BB did not change AP morphology and only insignificantly prolonged subendocardial APD from 323±24 ms to 345±18 ms (n=2), which confirmed our previous results in animals.[6] Because we do not have data from non-failing hearts, we can not exclude a different effect of BB in these hearts. However, based on the ECG data, it seems unlikely.

Histology

Histology and immunofluorescence experiments were performed as previously described.[5] After optical mapping experiments, human LV wedge preparations (n=10) were perfused with 3.7% formaldehyde for 5 minutes and left in the solution overnight. Then, the preparations were transferred to 20% sucrose for two days before the tissue was frozen. Wedge preparations were embedded in Tissue-Tek OCT compound (Histo Prep; Fisher Scientific, Fairlawn, NJ, USA), frozen in isopentane, and cryosectioned parallel to the epicardium. Tissue sections were mounted on Superfrost Plus glass slides (Fisher Scientific, Pittsburgh, PA) and maintained at −80°C until use. Sets of 16 μm cryosections were cut using a cryostat (Minitome Plus, TBS, Durham NC). Three different regions from the human LV preparation were sectioned parallel to the epicardial

surface: subepicardium (200-600 μm after the connective and epithelial tissue), mid-myocardium (at the middle of the depth), and subendocardium (200-600 μm after the connective and epithelial tissue and papillary muscle beginning). Sections were stained for histology with Masson's trichrome (International Medical Equipment, San Marcos, CA, USA). The examples of histological staining for subepicardial, midmyocardial, and subendocardial sections are presented on **Online Figure V A**.

Immunohistochemistry

In addition to histology, we used neighboring sister-sections for immunohistochemistry. Immunolabeling was carried out as described previously.[8, 9] Sections were stained with commercially available antibodies: Rabbit Cx43 (Sigma, 1:1000) and Mouse α-actinin (Sigma, 1:1600). Primary stains were applied overnight and then secondary antibodies were applied for 2.5 hours. Protein density was measured using the NIH ImageJ software as previously described.[5] Briefly, to quantitatively analyze the amount of Cx43 expression with respect to α-actinin, we obtained 20x images from the Nikon Confocal C1 microscope of 5 randomly selected fields of view in each area of myocardium: epi-, mid-, and endocardium. For each image, we used the ImageJ software with a thresholding macro to determine the ratio of connexin 43 to α-actinin.

Sets of 16 μm cryosections were cut using a cryostat. Three different regions from the human left ventricle preparation were sectioned parallel to the epicardial surface: subepicardium, midmyocardium, and subendocardium.

At least 3 different sections, from subepicardium, midmyocardium, and subendocardium regions, were double-stained for Cx43 and α-actinin with commercially-available antibodies. The following primary antibodies were applied overnight at 4°C: rabbit anti-Cx43 (Sigma, 1:1000) and mouse anti–α-actinin (sarcomere specific, Sigma, 1:1600). The following secondary antibodies were applied for 2 hrs at room temperature: Alexa Fluor 488 goat anti-rabbit IgG (Molecular Probes, 1:1000) and Alexa Fluor 555 goat anti-mouse IgG1 (Molecular Probes, 1:1000).

Protein density was measured using the ImageJ software (National Institute of Health) as previously described.[5] Briefly, to quantitatively analyze the amount of Cx43 expression with respect to α-actinin, we obtained 20x images from the Nikon Confocal C1 microscope of 5 randomly selected fields of view in each area of myocardium: subepi-, mid-, and subendocardium. For each image, we used the ImageJ software with a thresholding macro to determine the ratio of connexin 43 to α-actinin. A custom ImageJ Threshold macro was used to quantitatively analyze protein densities and ratios on immunohistochemistry slides fluorescently labeled with red and green secondary antibodies. Using the ImageJ interface, this program first split a fluorescently stained image into its three RGB

color channels. The user must manually identify in each RGB color channel signal and tissue threshold numbers (an intensity value between 0-255) to be used for each image selection. All pixels with intensity values equal to or above the threshold input values were included in the calculations. For this study, we set our signal threshold value based on ImageJ's AutoThreshold function as described previously.[5] Using ImageJ's Threshold function, we identified the threshold values which, when best combined, represented the entire tissue area. The tissue threshold input must be smaller than the signal threshold input value.

The threshold macro permitted the user to define the image selection(s) using three modes: Rectangle, ROI, or Rectangle ROI. Rectangle mode allowed the user to define a particular rectangular region of an image. It then broke up the output measurements into one row of sub-rectangular image-selections within this region. In ROI (Region of Interest) mode, the user could use ImageJ's selection tools (e.g. polygon and ellipse) and functions (AnalyzeParticle) to manually define particular image selection regions. The Rectangle ROI combined the Rectangle and ROI modes to create a pixilated overview of an entire image selection.

The threshold macro measures and outputs RGB Signal Area, Tissue Area, RGB Signal density, and RGB Signal Ratio values in each of the image selections. As previously described, each color channel's signal and tissue area were measured based off user input values. Signal density values were defined as a function of

each color channel's signal area divided by tissue area. RGB Signal Ratios were then calculated using each color channel's signal area.

Statistics

Comparisons between groups of data were performed using a t-test for non-paired measurements and nonparametric Kolmogorov-Smirnov test. A value of $p<0.05$ was considered statistically significant.

Reference List

1. Ueda N, Zipes DP, Wu J. Functional and transmural modulation of M cell behavior in canine ventricular wall. *Am J Physiol Heart Circ Physiol.* 2004;287:H2569-2575.

2. Voss F, Opthof T, Marker J, Bauer A, Katus HA, Becker R. There is no transmural heterogeneity in an index of action potential duration in the canine left ventricle. *Heart Rhythm.* 2009;6:1028-1034.

3. Fedorov VV, Kostecki G, Hemphill M, Efimov IR. Atria are more susceptible to electroporation than ventricles: implications for atrial stunning, shock-induced arrhythmia and defibrillation failure. *Heart Rhythm.* 2008;5:593-604.

4. Poelzing S, Dikshteyn M, Rosenbaum DS. Transmural conduction is not a two-way street. *J Cardiovasc Electrophysiol.* 2005;16:455.

5. Fedorov VV, Schuessler RB, Hemphill M, Ambrosi CM, Chang R, Voloshina AS, Brown K, Hucker WJ, Efimov IR. Structural and functional evidence for discrete exit pathways that connect the canine sinoatrial node and atria. *Circ Res.* 2009;104:915-923.

6. Fedorov VV, Lozinsky IT, Sosunov EA, Anyukhovsky EP, Rosen MR, Balke CW, Efimov IR. Application of blebbistatin as an excitation-contraction uncoupler for electrophysiologic study of rat and rabbit hearts. *Heart Rhythm.* 2007;4:619-626.

7. Glukhov AV, Flagg TP, Fedorov VV, Efimov IR, Nichols CG. Differential K(ATP) channel pharmacology in intact mouse heart. *J Mol Cell Cardiol.* 2009.

8. Fedorov VV, Glukhov AV, Sudharshan S, Egorov Y, Rosenshtraukh LV, Efimov IR. Electrophysiological mechanisms of antiarrhythmic protection during hypothermia in winter hibernating versus nonhibernating mammals. *Heart Rhythm.* 2008;5:1587-1596.

9. Hucker WJ, McCain ML, Laughner JI, Iaizzo PA, Efimov IR. Connexin 43 expression delineates two discrete pathways in the human atrioventricular junction. *Anat Rec (Hoboken).* 2008;291:204-215.

Figure and Table Legends

Online Table I. Patients' information. Group 1: Failing hearts.

Online Table II. Patients' information. Group 2: Non-Failing hearts.

Online Table III. The thickness of the LV wedge preparation (in mm).

Online Table IV. Transmural distribution of APD80% in non-failing (n=5) and failing (n=5) human hearts at different pacing cycle length.
The first part of the table represents APD80% values in different transmural areas: sub-epicardium, midmyocardium, sub-endocardium and in region with the longest APDs (Max). The second part of the table contains p-values for differences between non-failing and failing groups. Statistically significant changes are highlighted by red color.

Online Table V. P-values for transmural differences of APD80% in failing (n=5) and non-failing (n=5) human hearts at different pacing cycle length.
Statistically significant changes are highlighted by red color.

Online Figure I. Effect of the excitation-contraction uncoupler Blebbistatin in human ventricle.
The microelectrode recordings were used to validate the effect of Blebbistatin (10 μM) in the human left ventricle. The photo of the coronary perfused wedge

preparation in experimental the chamber is shown on A. Blebbistatin did not change action potential morphology (B), which confirms our previous results in animals. The microelectrode recordings are presented from the failing heart #1.

Online Figure II. Location of Max-APD islands.

Three examples from non-failing human hearts, where Max-APD islands were found, are presented. Data are shown from heart #1, #4, and #5 during pacing with cycle length 2,000 ms. Dotted line shows the region with APD within the top 30% range where local APD gradient threshold was applied and Max-APD islands were defined. To estimate size and area of Max-APD islands (brown areas on **panels C**), we used criteria based on the local APD gradient (**panels B**) with the threshold of 15 mm/ms. Maximum APD within this local APD gradient boundary line was identified and then used as a threshold for island with prolonged repolarization (shown on **panels C** for each example). Solid line on **panel C** shows the tissue border. It should be noticed that every heart had a individual size of the optical field of view which is shown by corresponding scales.

Online Figure III. Transmural APD distribution in all non-failing human hearts used in the study.

Online Figure IV. Transmural APD gradient in non-failing (A) and failing (B) human left ventricle wedge preparations.

Data are presented for non-failing hearts #2 and #4, and for failing hearts #3 and #4. Examples of activation and APD distribution patterns are plotted at CL=2000 ms. Next to APD distribution contour maps, corresponding examples of transmural APD distribution trough the marked cross sections are presented for the each heart. Time scales for APD distribution contour maps are identical for all hearts and amount to 130 ms with different range for the first heart (from 320 ms to 450 ms) against another hearts (from 410 ms to 540 ms). Transmural APD distributions are plotted in the same time range as corresponding APD distribution contour maps. Red dotted lines represent the maximum and minimum values of APD distribution through the transmural cross section. As shown on plots, local APD gradient was significantly bigger for non-failing hearts compared with failing hearts.

Online Figure V. Masson Trichrome staining of transmural sections from the human left ventricle.

A: Sample images from non-failing and failing human hearts taken from the subepicardium, midmyocardium, and subendocardium using a 10x magnification are presented. **B:** Average ratio of cardiac tissue to connective tissue throughout the hearts.

Online Table I. Patients' information. Group 1: Failing hearts.

Patient number	Sex	Age	Diagnosis	Device-base therapy	Pharmacological treatment
1	M	64	Nonischemic cardiomyopathy	AICD	Heparin, Beta, Statin, Inotrope
2	M	37	Dilated cardiomyopathy	AICD	ACE, ARB, Coumadin
3	M	28	Idiopathic cardiomyopathy	AICD, Biven PM	ACE, ARB, Coumadin, Inotropes
4	F	35	Restrictive cardiomyopathy	AICD, PM	ACE, ARB, Coumadin, Inotropes
5	M	61	Ischemic cardiomyopathy	AICD, PM	Beta, ACE, ARB, Coumadin, Inotropes

Online Table II. Patients' information. Group 2: Non-Failing hearts.

Patient number	Sex	Age	Diagnosis	Blood Pressure	Heart Rhythm, bpm	Ejection Fraction, %	Anamnesis
1	F	55	Death from stroke	112/56	101	20	RV function normal; Severely depressed LV systolic function; Dilated LV.
2	M	19	Brain Death from accident	145/87	130	45	Normal size heart; Acute cardiac Ischemia 32%; Atrial Fibrillation.
3	F	33	Death from Brain damage	120/80	94-140	25	——
4	M	68	Death from strock after surgery	110/60	70	65	Mild LV hyperdrophy; History: Prostate cancer
5	M	20	Death from overdose of Tylenol	——	——	——	——

Online Table III. The thickness of the LV wedge preparation (in mm).

Patient number	Non-Failing	Failing	
1	14.2	20.8	
2	21.9	19.1	
3	14.2	23.2	
4	15.7	14.1	
5	17.2	18.6	
average ± SEM	16.6 ± 1.4	19.2 ± 1.5	p=0.26

Online Table IV. Transmural distribution of APD80% in non-failing (n=5) and failing (n=5) human hearts at different pacing cycle length.

APD80% (ms)	4,000 ms *15 bpm*	2,000 ms *30 bpm*	1,000 ms *60 bpm*	750 ms *80 bpm*	500 ms *120 bpm*	300 ms *200 bpm*
Sub-Endo						
Non-Failing	510 ± 22	494 ± 22	437 ± 18	383 ± 21	316 ± 15	226 ± 9
Failing	516 ± 39	506 ± 35	450 ± 35	373 ± 21	305 ± 17	207 ± 10
Max						
Non-Failing	615 ± 45	537 ± 40	466 ± 25	410 ± 16	330 ± 12	228 ± 3
Failing	521 ± 30	495 ± 30	455 ± 34	379 ± 20	313 ± 11	215 ± 8
Mid						
Non-Failing	471 ± 21	455 ± 20	405 ± 16	362 ± 20	297 ± 12	216 ± 8
Failing	507 ± 32	495 ± 29	437 ± 31	367 ± 19	299 ± 13	206 ± 6
Sub-Epi						
Non-Failing	408 ± 21	383 ± 21	350 ± 16	316 ± 16	263 ± 12	196 ± 8
Failing	482 ± 25	477 ± 22	415 ± 18	357 ± 13	292 ± 9	196 ± 5
p-values (non-failing vs failing)						
Sub-Endo	0.907	0.779	0.756	0.758	0.644	0.285
Max	0.192	0.507	0.834	0.377	0.432	0.278
Mid	0.416	0.285	0.377	0.865	0.901	0.470
Sub-Epi	*0.031*	*0.014*	*0.029*	0.101	0.116	0.978

Online Table V. P-values for transmural differences of APD80% in failing and non-failing human hearts at different pacing cycle length.

Non-Failing Hearts (n=5)	4,000 ms *15 bpm*	2,000 ms *30 bpm*	1,000 ms *60 bpm*	750 ms *80 bpm*	500 ms *120 bpm*	300 ms *200 bpm*
Max						
vs Sub-Endo	*0.001*	*0.001*	*0.002*	*0.035*	0.080	0.432
vs Mid	*0.001*	*0.001*	*0.001*	*0.001*	*0.001*	*0.016*
vs Sub-Epi	*0.001*	*0.001*	*0.001*	*0.001*	*0.001*	*0.001*
Sub-Epi						
vs Sub-Endo	*0.025*	*0.006*	*0.007*	*0.035*	*0.026*	0.064
vs Mid	*0.040*	*0.037*	*0.044*	0.111	0.083	0.153
Failing Hearts (n=5)						
Max						
vs Sub-Endo	0.915	0.840	0.927	0.845	0.736	0.670
vs Mid	0.749	0.989	0.715	0.702	0.525	0.556
vs Sub-Epi	0.339	0.654	0.332	0.428	0.262	0.194
Sub-Epi						
vs Sub-Endo	0.482	0.512	0.406	0.583	0.585	0.453
vs Mid	0.559	0.644	0.547	0.709	0.712	0.367

Online Figure I

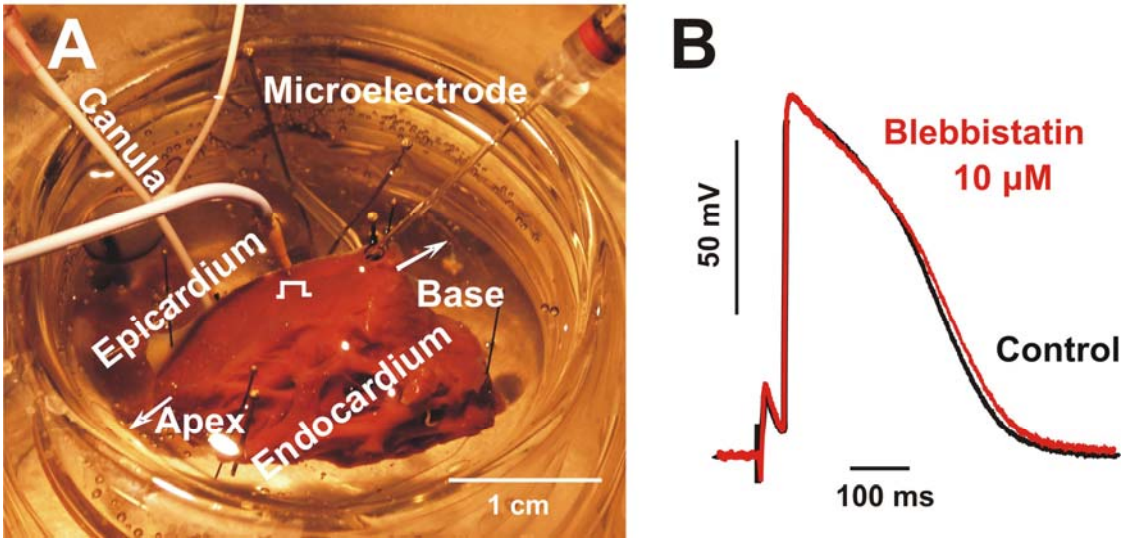

Online Figure II

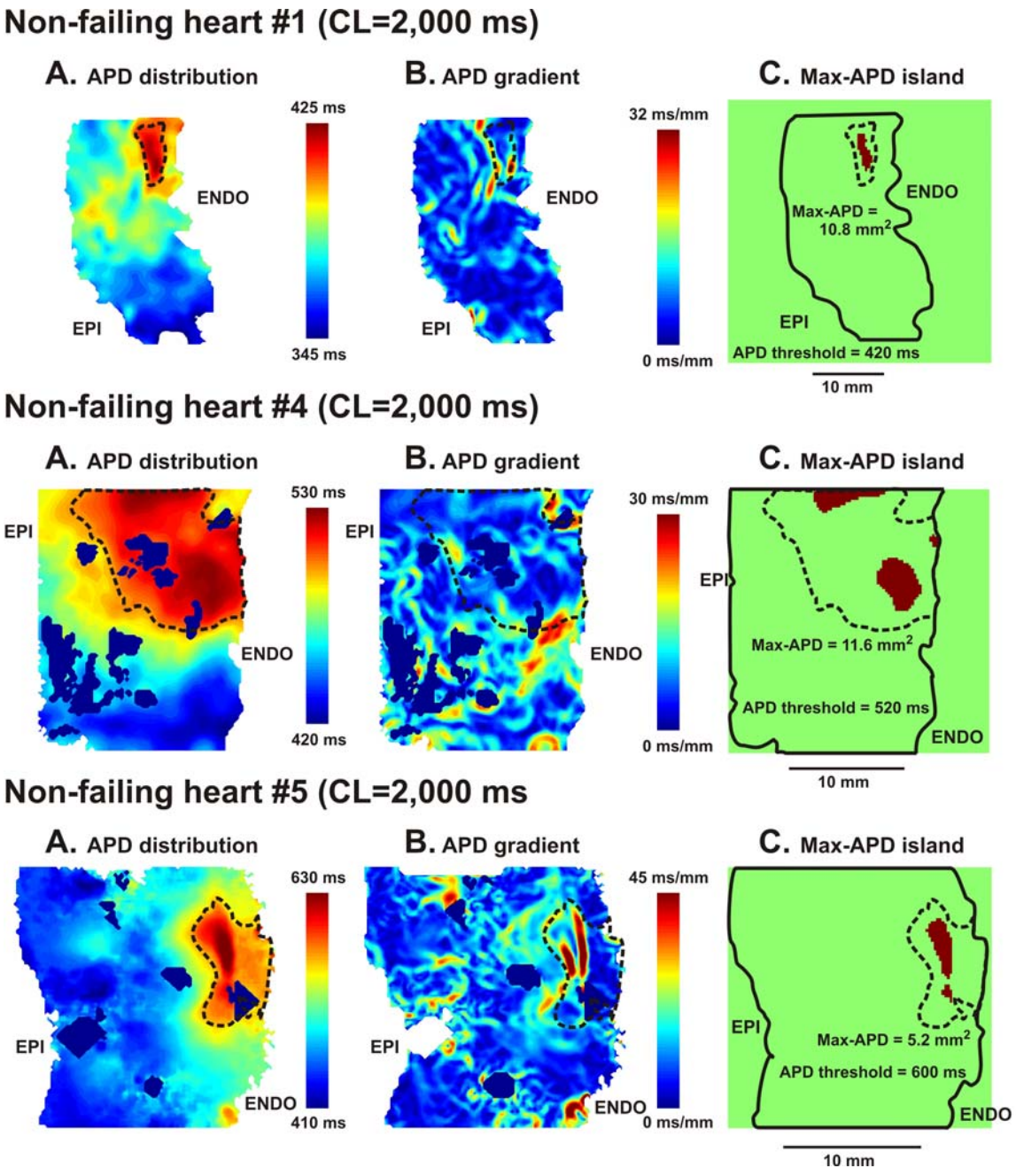

Online Figure III

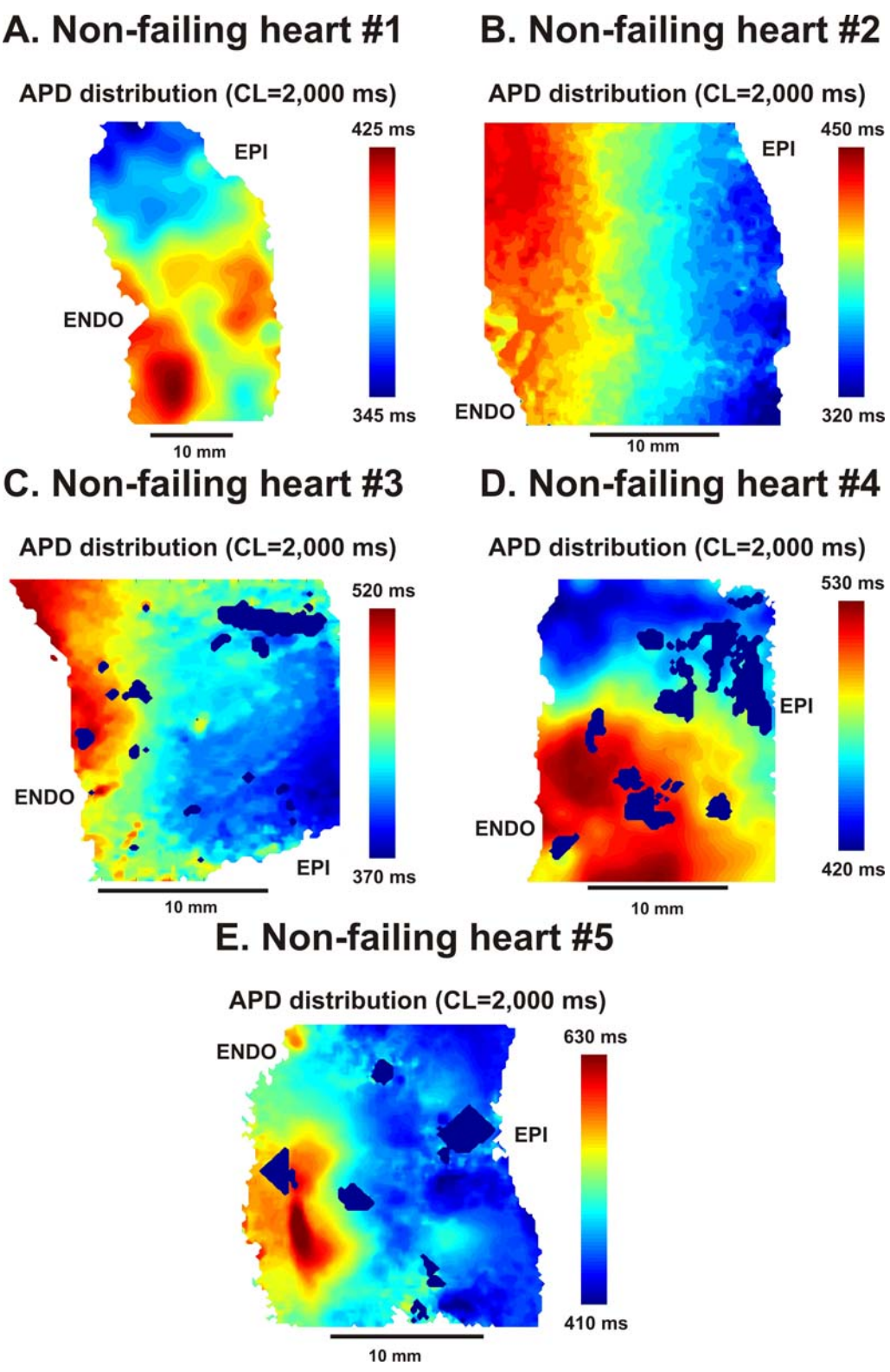

Online Figure IV

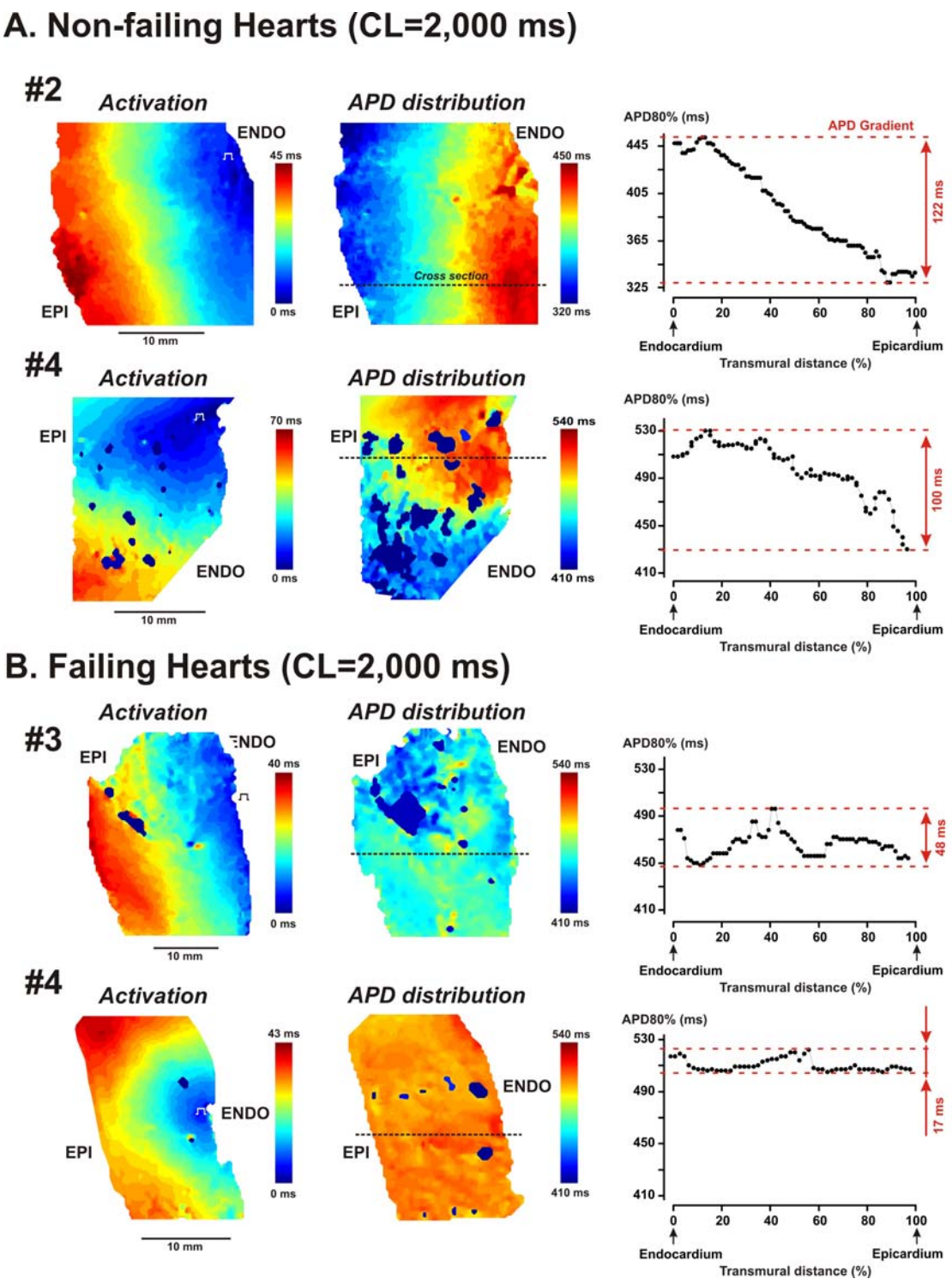

Online Figure V